YTUP

Journal of Thermal Engineering

https://jten.yildiz.edu.tr/

https://doi.org/10.47481/jten.0033

RESEARCH ARTICLE

Computation of compressible non-isothermal power-law model: developed Taylor-Galerkin / Pressure-correction method

Samah H. Al-Zaidi[1], Anas Al-Haboobi[2,*]

[1]Department of Mathematics, Faculty of Computer Sciences & Mathematics, University of Kufa, Kufa, 54001, Iraq
[2]Department of Mathematics, Faculty of Computer Sciences & Mathematics, University of Kufa, Kufa, 54001, Iraq

Abstract

In this study, a modified Taylor-Galerkin/pressure-correction finite-element approach has been developed to analyze non-isothermal, compressible, non-Newtonian, and inelastic fluid flows. In many cases, the coupling of viscosity and density to pressure and temperature is critical for accurate simulation of complex industrial and natural flows. The governing equations include the compressible Navier-Stokes system, the viscosity power-law model (for fluid rheology), and the Tait equation of state (to relate pressure and density). This important development is based on the integration of a two-step Lax-Wendroff method into the energy equation solver, enabling accurate thermal coupling and ensuring numerical stability. The novelty of this work lies in being the first to integrate compressibility, non-Newtonian viscosity, and non-isothermal effects into the Taylor-Galerkin/pressure-correction framework developed for power-law fluids. This integrated approach allows the simulation of high-fidelity, strongly coupled flow cases that are intractable for standard solvers. This provides a robust, approximate, and generalized method for higher-order problems in fluid mechanics, applicable to engineering or geophysical environments. The method's performance is assessed by investigating the influence of the power-law index, the consistency coefficient, the Prandtl number, and the thermal conductivity on the flow variables. The results show that, for a shear-thickening fluid, increasing the power-law index from 0.5 to 1.5 reduces the outlet velocity by 10%; by contrast, increasing the consistency coefficient from 1 (base case) to 20 raises the outlet velocity by up to 35% in both shear-thinning and shear-thickening scenarios. The centerline pressure increases with the consistency coefficient, and the density shows a similar trend. Thermal analysis indicates 22% increase in wall temperature under conditions of low thermal conductivity when the Prandtl number decreases from 1.4 to 0.6; however, the wall temperature increases rapidly in compressible, shear-thickening flows. Shear and normal stresses, which are elevated relative to those in a Newtonian fluid, can increase substantially (by 50%) as the power-law index and the consistency coefficient increase, indicating strong nonlinear rheological effects.

Keywords: Compressible flow, developed taylor-galerkin/pressure-correction method, non-isothermal flow, non-newtonian, power-law model

Cite this article as: Al-Zaidi, S. H., & Al-Haboobi, A. (2026). Computation of compressible non-isothermal power-law model: developed Taylor-Galerkin /Pressure-correction method. Journal of Thermal Engineering, 12(4), 1337–1349. https://doi.org/10.47481/jten.0033

1. Introduction

Non-Newtonian fluids constitute an important class in fluid dynamics, with relevance spanning theoretical understanding and practical applications across multiple industries. The non-constant viscosity of these materials, which includes sauces, blood and polymeric solutions is responsible for flow behaviors that are drastically more complex than the behavior of Newtonian fluids [1-4]. Such complexity is particularly relevant to engineering, biomedical, and environmental fields, which can benefit from more accurate representations of fluid dynamics and thereby improve their design processes and operational performance. Thus, the study of non-Newtonian fluids remains an area of considerable research interest. As another example, [5,6] investigate atomization processes for non-Newtonian fluids and [7–10] consider the gas bubbles behaviors within a non-Newtonian liquid matrix. In recent years, there has been growing scholarly interest in the study of Casson fluids. The Casson fluid belongs to a class of non-Newtonian fluids with generalized Newtonian behavior usually associated with the presence of a yield stress, and in recent times it has received increased attention from scholars due to its particular

*Corresponding Author
E-mail Adress: anasm.ali@uokufa.edu.iq

Submitted: 17 February 2025 ; **Accepted:** 31 May 2025

This paper was recommended for publication in revised form by Editor-in-Chief Ahmet Selim Dalkılıç

relevance for many biomedical and industrial applications (cf., e.g., [11-20]).

The behavior of non-isothermal, non-Newtonian fluids play a pivotal role in a wide range of industrial and engineering applications, such as polymer processing, geothermal flows, food manufacturing, and biomedical systems. In these contexts, the interaction between momentum and thermal transport mechanisms is strongly influenced by the fluid's rheological properties, particularly when nonlinear viscosity effects are present. While significant research has been conducted on the heat transfer characteristics of such fluids, especially through numerical modeling [21-26], most existing work assumes isothermal or incompressible flow conditions, which simplifies the thermodynamic and constitutive complexities of real systems. One of the most successful, widely applied, and accurate numerical solution methods for these important fluid problems, namely Taylor-Galerkin/Pressure-Correction (TG/PC) is primarily limited to the finite element method (FEM). This approach, introduced by Townsend and Webster [27], has been extensively used to solve a variety of fluid-related problems, primarily at isothermal conditions. For examples of such research, Tamaddon-Jahromi, et. al, [28] used Taylor–Galerkin algorithms for solving model convection–diffusion problems for simulating more complex non-Newtonian flows. Carew, et. al, are solved a viscoelastic flow using TG/PC method that incorporates consistent Petrov-Galerkin streamline upwinding within the discretisation of the constitutive equations [29]. A semi-implicit TG/PC was developed to investigate problems that manifest free surfaces associated with the incompressible Newtonian fluids by Ngamaramvaranggul and Webster [30]. [31] TG/PC method was used for solving die-swell flow for viscoelastic and viscoelastoplastic fluids by Al-Muslimawi. Sharhan and Al-Muslimawi [32] had examine the flow of inelastic fluids with various shear properties by TG/PC algorithm. Al-Haboobi, et. al used TG/PC for first time to study a Newtonian isothermal flow around bluff body for incompressible [33] and compressible fluid [34].

A major limitation in the open literature is the lack of high-fidelity numerical methods capable of simulating compressible, non-isothermal, non-Newtonian fluids, particularly those described by the power-law model. Existing studies have primarily addressed either incompressible non-Newtonian flows or compressible Newtonian flows. Challenges arise from the nonlinear coupling among temperature, viscosity, pressure, and density, and from the need to simultaneously solve the energy equation and a pressure-density relation, such as the Tait equation of state.

To fill this research gap, Al-Haboobi and Al-Muslimawi proposed in 2023 a new method for non-isothermal compressible Newtonian fluids, namely the developed Taylor-Galerkin/Pressure-Correction (DTG/PC) method [35]. It solves the energy equation using a two-step Lax-Wendroff scheme and applies a pressure correction for compressibility based on the Tait equation of state. Its application to more complex constitutive laws, specifically those described by the power-law model for non-Newtonian fluids, has not yet been examined.

The current work is based on this framework, but extends the earlier works by providing, for the first time, a generalized extension of the DTG/PC method to model non-isothermal, compressible, inelastic fluids governed by an Ostwald-de Waele power-law fluid law [36]. This model is able to capture both shear-thinning and shear-thickening behavior by varying the power-law index (n) and consistency coefficient (m). With the Tait equation accounting for compressibility and the energy equation allowing for thermal coupling, a fully coupled, thermodynamically consistent model is achieved.

To validate the robustness of the proposed methodology, we conducted a detailed numerical investigation in an axisymmetric cylindrical channel. The effects of key physical parameters (n), (m), (k), Pr namely the power-law index, the consistency parameter, the thermal conductivity, and the Prandtl number on important flow variables (axial velocity (v), pressure (p), density (ρ), temperature (T), shear stress (τ_{rz}), and normal stress (τ_{zz}) are analyzed.

The originality of this study lies in extending the DTG/PC framework to compressible, non-isothermal power-law fluids, which has not been reported in the literature. The method captures the complex thermodynamic-rheological coupling and produces stable, high-fidelity evolution. This gap is addressed by providing a robust numerical infrastructure for simulating complex flows essential to diverse scientific and industrial applications.

2. Mathematical description

The continuity, momentum, and energy equations that govern non-isothermal, compressible, inelastic, flow are expressed in two-dimensional cylindrical coordinates (r, z) respectively, as [34, 35]:

Conservation of mass

$$\frac{\partial \rho}{\partial t} + \nabla \cdot (\rho v) = 0 \qquad (1)$$

In component form:

$$\frac{\partial \rho}{\partial t} + \frac{1}{r}\frac{\partial (\rho r v_r)}{\partial r} + \frac{\partial (\rho v_z)}{\partial z} = 0 \qquad (2)$$

Conservation of momentum:

$$\rho\left(\frac{\partial ev}{\partial t} + (v.\nabla)v\right) = \nabla(2\mu_s d) - \frac{2}{3}\nabla(\mu_s \nabla.v) - \nabla p. \qquad (3)$$

In component form:

r-direction

$$\frac{\partial v_r}{\partial t} + v_r\frac{\partial v_r}{\partial r} + v_z\frac{\partial v_r}{\partial z} = -\frac{1}{\rho}\frac{\partial p}{\partial r} + \frac{1}{\rho}\frac{\partial}{\partial r}\left[\mu_s\left(-\frac{2}{3}\nabla\cdot v + 2\frac{\partial v_r}{\partial r}\right)\right] + \frac{1}{\rho}\frac{\partial}{\partial z}\left[\mu_s\left(\frac{\partial v_r}{\partial z} + \frac{\partial v_z}{\partial r}\right)\right] + \frac{1}{\rho}\frac{2\mu_s}{r}\left(\frac{\partial v_r}{\partial r} - \frac{v_r}{r}\right),$$

(4)

z-direction

$$\frac{\partial v_z}{\partial t}+v_r\frac{\partial v_z}{\partial r}+v_z\frac{\partial v_z}{\partial z}=-\frac{1}{\rho}\frac{\partial p}{\partial r}+\frac{1}{\rho}\frac{\partial}{\partial z}\left[\mu_s\left(-\frac{2}{3}\nabla\cdot v+2\frac{\partial v_z}{\partial z}\right)\right]+\frac{1}{\rho}\frac{\partial}{\partial r}\left[\mu_s\left(\frac{\partial v_z}{\partial r}+\frac{\partial v_r}{\partial z}\right)\right]+\frac{1}{\rho}\frac{\mu_s}{r}\left(\frac{\partial v_r}{\partial z}+\frac{\partial v_z}{\partial r}\right). \quad (5)$$

Conservation of energy

$$\rho C_p\left[\frac{\partial T}{\partial t}+(v.\nabla)T\right]=\nabla.(k\nabla T)+\Phi. \quad (6)$$

In component form:

$$\rho C_p\left[\frac{\partial T}{\partial t}+v_r\frac{\partial T}{\partial r}+v_z\frac{\partial T}{\partial z}\right]=\frac{1}{r}\frac{\partial}{\partial r}\left(kr\frac{\partial T}{\partial t}\right)+\frac{\partial}{\partial z}\left(k\frac{\partial T}{\partial z}\right)+\Phi. \quad (7)$$

Where $v=(v_r,v_z)$, p, ρ and μ_s are the velocity vector, pressure, density, and solvent viscosity of the fluid, respectively. In the energy equation, the two variables each represent the temperature T, the heat capacity C_p, the thermal conductivity k, and the dissipation function Φ. The deformation tensor's Euler rate is defined as follows. $d=(\nabla v+(\nabla v)^{\dagger})/2$. The solvent viscosity is calculated using a power-law model, which is defined as [32]:

$$\mu_s=m(\gamma)^{n-1} \quad (8)$$

Where, m is consistency parameter, n is power-law index and γ represent the shear rate of simple shear flow defined as [32]:

$$\gamma=2\sqrt{II}. \quad (9)$$

Where, II denotes the second invariants of the rate of strain tensor, which can be articulated in an axisymmetric coordinate system as follows [32]:

$$II=\frac{1}{2}\left\{\left(\frac{\partial v_r}{\partial r}\right)^2+\left(\frac{\partial v_z}{\partial z}\right)^2+\left(\frac{v_r^2}{r}\right)+\frac{1}{2}\left(\frac{\partial v_r}{\partial r}+\frac{\partial v_z}{\partial z}\right)^2\right\}. \quad (10)$$

To non-dimensionalize the conservation (of mass, momentum and energy), we have used the following variables:

$$v=V^0v^*,\rho=\rho^0\rho^*,p=\frac{\mu_sV^0}{L}p^*,T=\frac{T-T_0}{\Delta T},\nabla=\frac{1}{L}\nabla^*,t=\frac{L^2\rho^0}{\mu_s}t^*,$$

where V^0 is the characteristic velocity, p^0 is the characteristic pressure, ρ^0 is the characteristic density, T^0 is the characteristic temperature, L is the characteristic length, and ΔT is a difference reference temperature.

Using the quantities defined above, Equations 1 through 6 can be transformed into the following equations: Conservation of mass

$$\frac{\partial\rho}{\partial t}+\mathrm{Re}\,\nabla\cdot(\rho v)=0. \quad (11)$$

In component form:

$$\frac{\partial\rho}{\partial t}+\mathrm{Re}\left(\frac{1}{r}\frac{\partial(\rho rv_r)}{\partial r}+\frac{\partial(\rho v_z)}{\partial z}\right)=0. \quad (12)$$

Conservation of momentum:

$$\rho\,\mathrm{Re}\left(\frac{\partial v}{\partial t}+(v.\nabla)v\right)=\nabla(2\mu_s d)-\frac{2}{3}\nabla(\mu_s\nabla.v)-\nabla p. \quad (13)$$

In component form:

r-direction

$$\frac{\partial v_r}{\partial t}+v_r\frac{\partial v_r}{\partial r}+v_z\frac{\partial v_r}{\partial z}=-\frac{1}{\rho}\frac{1}{\mathrm{Re}}\frac{\partial p}{\partial r}+\frac{1}{\rho}\frac{1}{\mathrm{Re}}\frac{\partial}{\partial r}\left[\mu_s\left(-\frac{2}{3}\nabla\cdot v+2\frac{\partial v_r}{\partial r}\right)\right]+\frac{1}{\rho}\frac{1}{\mathrm{Re}}\frac{\partial}{\partial z}\left[\mu_s\left(\frac{\partial v_r}{\partial z}+\frac{\partial v_z}{\partial r}\right)\right]+\frac{1}{\rho}\frac{1}{\mathrm{Re}}\frac{2\mu_s}{r}\left(\frac{\partial v_r}{\partial r}-\frac{v_r}{r}\right), \quad (14)$$

z-direction

$$\frac{\partial v_z}{\partial t}+v_r\frac{\partial v_z}{\partial r}+v_z\frac{\partial v_z}{\partial z}=-\frac{1}{\rho}\frac{1}{\mathrm{Re}}\frac{\partial p}{\partial z}+\frac{1}{\rho}\frac{1}{\mathrm{Re}}\frac{\partial}{\partial z}\left[\mu_s\left(-\frac{2}{3}\nabla\cdot v+2\frac{\partial v_z}{\partial z}\right)\right]+\frac{1}{\rho}\frac{1}{\mathrm{Re}}\frac{\partial}{\partial r}\left[\mu_s\left(\frac{\partial v_z}{\partial r}+\frac{\partial v_r}{\partial z}\right)\right]+\frac{1}{\rho}\frac{1}{\mathrm{Re}}\frac{\mu_s}{r}\left(\frac{\partial v_z}{\partial z}+\frac{\partial v_r}{\partial r}\right). \quad (15)$$

Conservation of energy

$$\rho\,\mathrm{RePr}\left[\frac{\partial T}{\partial t}+(v.\nabla)T\right]=\nabla.(k\nabla T)+\mathrm{Pr}\,\mathrm{Ec}\Phi. \quad (16)$$

In component form:

$$\rho\,\mathrm{Re}\,\mathrm{Pr}\left[\frac{\partial T}{\partial t}+v_r\frac{\partial T}{\partial r}+v_z\frac{\partial T}{\partial z}\right]=\frac{1}{r}\frac{\partial}{\partial r}\left(kr\frac{\partial T}{\partial t}\right)+\frac{\partial}{\partial z}\left(k\frac{\partial T}{\partial z}\right)+\mathrm{Pr}\,\mathrm{Ec}\Phi. \quad (17)$$

Where Re, Pr and Ec are non-dimensional values representing the Reynolds number, Prandtl number, and Eckert number, respectively, defined as [35,37]:

$$\mathrm{Re}=\frac{\rho^0V^0L}{\mu_s},$$

$$\mathrm{Pr}=\frac{\mu_s}{k/C_p},$$

$$\mathrm{Ec}=\frac{(V^0)^2}{C_p\Delta t}$$

Then, we need to specify an equation of state — a relation between density and pressure — to close the two governing equations (mass and momentum) outlined above. The modified Tait of state equation has been assumed in the form [38]:

$$\frac{p + B}{p_0 + B} = (\frac{\rho}{\rho_0})^A, \tag{18}$$

Here A and B represent parameters, and denote p^0, ρ^0 the reference values of pressure and density, respectively.

By rearranging and differentiating Equation 18, we obtain:

$$\frac{\partial p}{\partial \rho} = A\alpha\rho^{A-1} = \frac{A(p + B)}{\rho} = c^2_{(x,t)} \tag{19}$$

Where, $\alpha = \frac{(p^0 + B)}{\rho_0^A}$ is constant and $c_{(x,t)}$ is the speed of sound.

3. Numerical algorithm

In this section, we discuss the DTG/PC method, which is used to solve the governing equations for compressible non-Newtonian fluids with thermal effects. The algorithm employs the Taylor-Galerkin technique, a fractional-step method that initially semi-discretizes time using a Taylor series expansion, and subsequently applies a pressure-correction approach. This numerical strategy was first introduced by Hawken et al. [27] to address incompressible isothermal flows. Subsequently, the Lax-Wendroff two-step [39] procedure was applied to the preceding equations and to derive the following results.

Momentum conservation equation becomes:

$$\begin{aligned} &\text{step1: } v^{n+1/2} = v^n + \frac{\Delta t}{2\rho\,Re}(\quad (v^n, d^n) - \nabla p^n), \\ &\text{step2: } v^{n+1} = v^n + \frac{\Delta t}{\rho\,Re}(\quad (v^{n+1/2}, d^{n+1/2}) - \nabla p^{n+1/2}), \end{aligned} \tag{20}$$

where,

$$(v, d) = \nabla\,(2\mu_s d) - \frac{2}{3}\nabla\,(\mu_s \nabla \cdot v) - \rho\,Re\,(v \cdot \nabla)\,v. \tag{21}$$

In step 2 of Equation 20, we approximate pressure $p^{n+1/2}$ by using Crank-Nicolson method as [40]:

$$p^{n+1/2} = \vartheta p^{n+1} + (1 + \vartheta)\,p^n \tag{22}$$

Now using Equation 22 we can re - written step 2 of Equation 20 as:

$$v^{n+1} = v^n + \frac{\Delta t}{\rho\,Re}(\quad (v^{n+1/2}, d^{n+1/2}) - \vartheta\nabla p^{n+1} - (1 - \vartheta)\nabla p^n). \tag{23}$$

The velocity v^* introduce to solve Equation 23 in conjugation with the compressibility Equation 11, as:

$$v^* = v^n + \frac{\Delta t}{\rho\,Re}(\quad (v^{n+1/2}, d^{n+1/2}) - \nabla p^n). \tag{24}$$

Now by subtracting Equation 24 from Equation 23 we have

$$v^{n+1} = v^* - \frac{\vartheta\Delta t}{\rho Re}\nabla q^{n+1}, \quad q^{n+1} = p^{n+1} - p^n \tag{25}$$

Taking the divergence of both sides of Equation 25 together with using Equation 11

$$\frac{\Delta\rho^{n+1}}{\Delta t} + \nabla \cdot (\rho\,Re\,v^*) = \vartheta\Delta t\nabla^2 q^{n+1} \tag{26}$$

Moreover, by applying the chain rule to Equation 19 and performing difference operations, the density increment can be expressed in terms of the pressure increment,

$$\frac{\Delta\rho^{n+1}}{\Delta t} = \frac{1}{c^2_{(x,t)}}\frac{\Delta p^{n+1}}{\Delta t}. \tag{27}$$

Substituting Equation 27 in to Equation 26 we get

$$\frac{1}{c^2_{(x,t)}}\frac{\Delta p^{n+1}}{\Delta t} + \nabla \cdot (\rho\,Re\,v^*) = \vartheta\Delta t\nabla^2 q^{n+1}. \tag{28}$$

Now, we get the energy conservation equation:

$$\begin{aligned} &\text{step1:} \quad T^{n+1/2} = T^n + \frac{\Delta t}{2\rho\,RePr}(G(v^n, T^n), \\ &\text{step2:} \quad T^{n+1} = T^n + \frac{\Delta t}{\rho\,RePr}(G(v^{n+1/2}, T^{n+1/2}), \end{aligned} \tag{29}$$

where,

$$G(v, T) = \nabla \cdot (k\nabla T) - \rho\,RePr\,(v \cdot \nabla)\,Pr\,Ec\Phi.$$

Thus, from Equation (20 step 1), and Equations 24, 25, 27, 28, 29, we can solve the system of compressible non-Newtonian inelastic equations at the following stages:

$$\text{stage1:} \quad v^{n+1/2} = v^n + \frac{\Delta t}{2\rho^n Re}(\quad (v^n, d^n) - \nabla p^n), \tag{30}$$

$$\text{stage2:} \quad T^{n+1/2} = T^n + \frac{\Delta t}{2\rho^n RePr}(G(v^n, T^n)), \tag{31}$$

$$\text{stage3:} \quad v^* = v^n + \frac{\Delta t}{\rho^n Re}(\quad (v^{n+1/2}, d^{n+1/2}) - \nabla p^n), \tag{32}$$

$$\text{stage4:} \quad T^{n+1} = T^n + \frac{\Delta t}{\rho^n RePr}(G(v^{n+1/2}, T^{n+1/2})), \tag{33}$$

$$\text{stage5:} \quad \frac{1}{c^2_{(x,t)}}\frac{\Delta p^{n+1}}{\Delta t} + \nabla \cdot (\rho^n\,Re\,v^*) = \vartheta\Delta t\nabla^2 q^{n+1}, \tag{34}$$

$$\text{stage6:} \quad \frac{\Delta\rho^{n+1}}{\Delta t} = \frac{1}{c^2_{(x,t)}}\frac{\Delta p^{n+1}}{\Delta t}, \tag{35}$$

$$\text{stage7:} \quad v^{n+1} = v^* - \frac{\vartheta\Delta t}{\rho^n Re}\nabla q^{n+1}. \tag{36}$$

Now, these stages can be described in matrix/vector form as follows:

$$\text{stage1:} \quad \frac{2\rho^n \mathrm{Re}}{\Delta t}\mathfrak{M}\Delta V^{n+1/2} = \mathfrak{L}^{\dagger} P^n - \mathfrak{S}V^n + \frac{2}{3}\mathfrak{D}V^n - \rho^n \mathrm{Re}\,\mathfrak{N}(V^n)V^n + \mathfrak{B}, \tag{37}$$

$$\text{stage2:} \quad \frac{2\rho^n \mathrm{RePr}}{\Delta t}\mathfrak{M}\Delta T^{n+1/2} = -\mathfrak{C}T^n - \rho^n \mathrm{RePr}\,\mathfrak{N}(T^n)V^n + \mathfrak{B} + \mathrm{Pr}\,\mathrm{Ec}\Phi, \tag{38}$$

$$\text{stage3:} \quad \frac{\rho^n \mathrm{Re}}{\Delta t}\mathfrak{M}\Delta V^{*} = \mathfrak{L}^{\dagger} P^n - \mathfrak{S}V^{n+1/2} + \frac{2}{3}\mathfrak{D}V^{n+1/2} - \rho^n \mathrm{Re}\,\mathfrak{N}(V^{n+1/2})V^{n+1/2} + \mathfrak{B}, \tag{39}$$

$$\text{stage4:} \quad \frac{\rho^n \mathrm{RePr}}{\Delta t}\mathfrak{M}\Delta T^{n+1} = -\mathfrak{C}T^{n+1/2} - \rho^n \mathrm{RePr}\,\mathfrak{N}(T^{n+1/2})V^{n+1/2} + \mathfrak{B} + \mathrm{Pr}\,\mathrm{Ec}\Phi, \tag{40}$$

$$\text{stage5:} \quad \frac{1}{c^2_{(x,t)}}\frac{1}{\Delta t}\mathfrak{H}\Delta p^{n+1} + \rho^n \mathrm{Re}\,\mathfrak{B}V^{*} = -\vartheta\Delta t\mathfrak{K}\mathfrak{Q}^{n+1}, \tag{41}$$

$$\text{stage6:} \quad \frac{1}{\Delta t}\mathfrak{H}\Delta\rho^{n+1} = \frac{1}{c^2_{(x,t)}}\frac{1}{\Delta t}\mathfrak{H}\Delta p^{n+1}, \tag{42}$$

$$\text{stage7:} \quad \frac{\mathrm{Re}}{\Delta t}\mathfrak{M}\Delta V^{n+1} = \vartheta\mathfrak{L}^{\dagger}\mathfrak{Q}^{n+1}, \tag{43}$$

where, $\Delta V^{n+1/2} = V^{n+1/2} - V^n$, $\Delta V^{n+1} = V^{n+1} - V^{*}$, $\Delta T^{n+1/2} = T^{n+1/2} - T^n$, $\Delta T^{n+1} = T^{n+1} - T^n$, $\Delta p^{n+1} = p^{n+1} - p^n$, $\Delta\rho^{n+1} = \rho^{n+1} - \rho^n$ and $\Delta V^{*} = V^{*} - V^n$.

V, T, ρ, and P represent a velocity, energy, density, and pressure vector, respectively. The vector of pressure difference is defined as $\mathfrak{Q}^{n+1} = P^{n+1} - P^n$.

The notation and structure of the matrix are delineated as follows:

$$\mathfrak{M}_{ij} = [\Lambda_i, \Lambda_j] = \int_{\Omega} \Lambda_i \Lambda_j d\Omega \qquad \mathfrak{L}_{ij} = (\psi_i, \nabla\cdot\Lambda_j) = \int_{\Omega} \psi_i \nabla\cdot\Lambda_j d\Omega$$

$$\mathfrak{S}_{ij} = \langle \nabla\Lambda_i, \nabla\Lambda_j + (\nabla\Lambda_j)^{\dagger}\rangle = \int_{\Omega} \mu_s \nabla\Lambda_i : (\nabla\Lambda_j + (\nabla\Lambda_j)^{\dagger})\, d\Omega$$

$$\mathfrak{D}_{ij} = [\nabla\Lambda_i, \nabla\Lambda_j] = \int_{\Omega} \mu_s \nabla\Lambda_i \cdot \nabla\Lambda_j d\Omega, \quad \mathfrak{K}_{ij} = [\nabla\psi_i, \nabla\psi_j] = \int_{\Omega} \nabla\psi_i \cdot \nabla\psi_j d\Omega$$

$$\mathfrak{H}_{i,j} = (\psi_i, \psi_j) = \int_{\Omega} \psi_i \psi_j d\Omega, \quad \mathfrak{B}_{ij} = (\psi_i, \nabla\cdot(\psi_j\Lambda_j)) = \int_{\Omega} \psi_i \nabla\cdot(\psi_j\Lambda_j) d\Omega$$

$$\mathfrak{N}(T)_{ij} = [\Lambda_i, T\cdot\nabla\Lambda_j] = \int_{\Omega} \Big(\sum\nolimits_l \Lambda_i \Lambda_j T^l \cdot \nabla\Big)\Lambda_j d\Omega$$

$$\mathfrak{N}(V)_{ij} = [\Lambda_i, \mathbf{V}\cdot\nabla\Lambda_j] = \int_{\Omega} \Big(\sum\nolimits_l \Lambda_i \Lambda_j V^l \cdot \nabla\Big)\Lambda_j d\Omega$$

$$\mathfrak{C}_{ij} = [\nabla\Lambda_i, \nabla\Lambda_j] = \int_{\Omega} \alpha\nabla\Lambda_i \cdot \nabla\Lambda_j d\Omega, \quad \mathfrak{B}_i = [\Lambda_i, g]_{\Gamma} = \int_{\Gamma} g\cdot\Lambda_i d\Gamma$$

where $\mathfrak{B}$, g are a natural boundary vector and given function. We approximate the values of velocity, pressure, and temperature as follows: $v = \sum_i v^i(t)\Lambda_i, T = \sum_i T^i(t)\Lambda_i$ and $p = \sum_j \psi_j p$. Λ_i and ψ_j represent the quadratic and linear shape function respectively.

4. Specification of the problem and boundary conditions

We investigate the compressible Poiseuille flow (Ps) through a straight, two-dimensional (2D) axisymmetric channel under non-isothermal conditions. We use a highly refined triangular finite-element mesh with a normal junction-configuration, as shown in Figure 1. The mesh comprises 1679 elements, 960 vertices, and 3840 degrees of freedom.

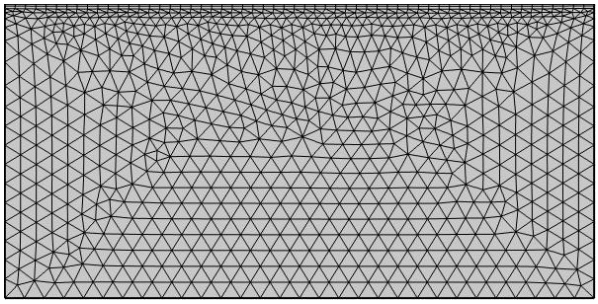

Figure 1. Structured finite element mesh

The boundary conditions necessary to solve the problem are setting as follow:

1. At the channel inlet, a prescribed temperature and a fully developed axial velocity profile corresponding to Poiseuille (Ps) flow are imposed.
2. Along the axisymmetric, we assume no slip boundary condition for velocity.
3. Along the channel wall, we assume constant heat flux for temperature, $\frac{\partial T}{\partial r} = q_1$, where q_1 is constant.

The above details are depicted in Figure 2.

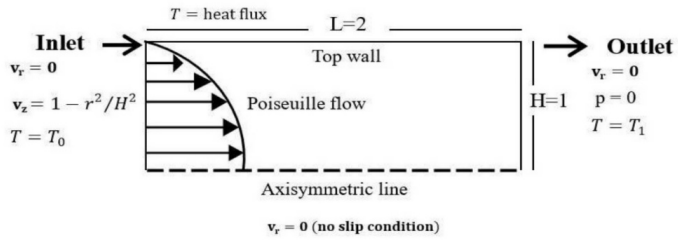

Figure 2. The flow problem's geometry boundary conditions

5. Results and discussions

In the present work, we performed systematic simulations of steady, non-Newtonian thermal flow using the DTG/PC method, an advanced and efficient numerical technique. The main purpose of this study is to investigate the impact of the power-law index (n) and the consistency parameter (m) on flow characteristics and to discuss the effect of the Prandtl number (Pr) and the thermal conductivity (k) on temperature. Such studies are performed for individual values $(n = 0.5 \text{ to} 1.5)$ of $(m = 1, 5, 10, 20)$ and, to illustrate the range of flow behaviour under varying thermal and rheological conditions.

5.1. Velocity profile with n and m variation

We analyze the effects of power-law index (n) and consistency parameter (m) on fluid velocity at both inlet and outlet of the channel. Within this range, the power-law index is changed between $0.5 \leq n \leq 1.5$ with steps of , and everything else is kept constant (e.g. Pr=m=1). The effect of the variation of on velocity profile at channel entrance is presented in Figure 3. As expected, and confirmed as found above, there is no significant effect. This behavior is result of the impact of the boundary conditions (those in Figure 2).

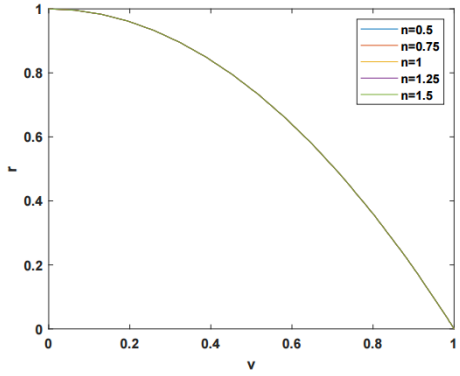

Figure 3. Influence of variation n on velocity at inlet

The conduit outlet's behavior differs markedly and apparently affects local velocity. As shown in Figure 4, for sufficiently large values of the independent variable, the velocity slightly n<1 increases, which resembles shear-thinning behavior. In contrast, increasing the n > 1 value yields a small decrease in velocity, characteristic of shear-thickening behavior.

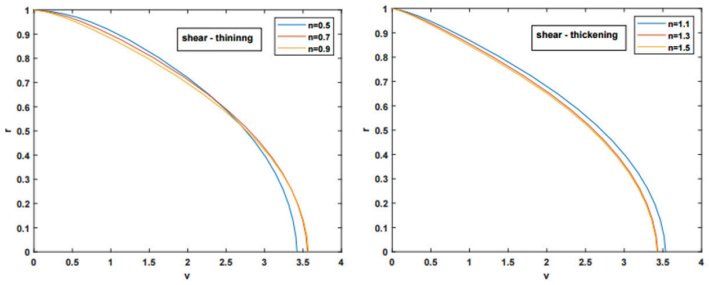

Figure 4. Influence of variation n on velocity at outlet

We investigate the effects of varying the consistency coefficient (m) at values of 1, 5, 10, and 20, for both shear-thinning (n=0.5) and shear-thickening (n=1.5) fluids, while keeping all other parameters constant (Re=Pr=1). Figure 5 shows that increasing the consistency

coefficient (m) does not affect the inlet velocity profile. This behavior is a consequence of the dominant influence of the inlet boundary conditions, as illustrated in Figure 2.

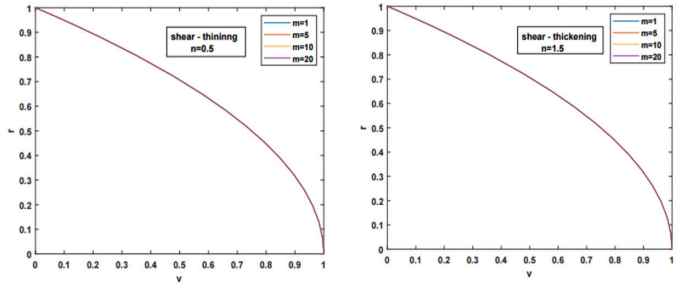

Figure 5. Influence of variation m on velocity at inlet

At the channel outlet, the effect of varying the consistency coefficient is examined using the results presented in Figure 6. The figure demonstrates that increasing m leads to a pronounced rise in velocity relative to that at the channel inlet. Furthermore, it is observed that the influence of increasing m on velocity is more pronounced for power-law index values, which is n < 1 attributed to the shear-thinning behavior of the fluid. Everything that has been mentioned up until this point is consistent with what was provided in [35, 41].

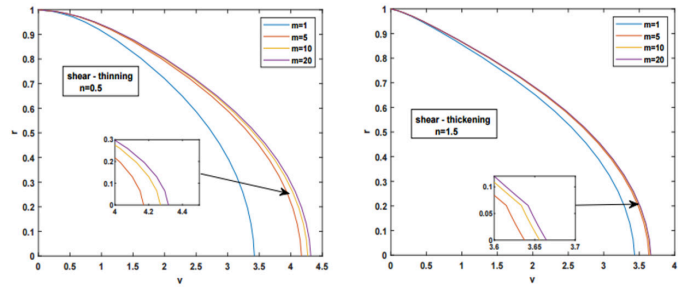

Figure 6. Influence of variation m on velocity at outlet

Figure 7 shows the centerline pressure (p) and density (ρ) profiles for different values of the power-law index (n), illustrating pressure- and density-drop profiles as n and m vary. Here we can see the results of ρ and p distribution for maximum values (n=1.5) These observations are consistent with the known physical behaviour of non-Newtonian fluids. Decreasing n increases the fluid's viscosity (its resistance to flow). Thus, this results in increased pressure and density at the same flow condition [35, 42].

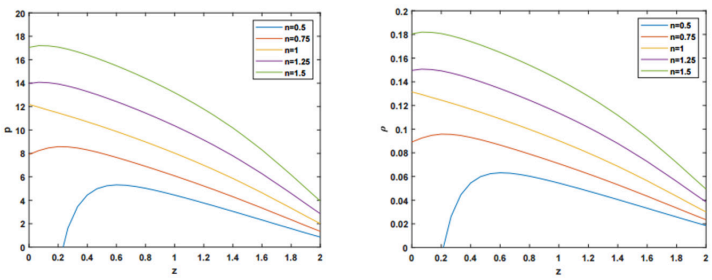

Figure 7. Influence of variation n on pressure and density

The influence of the consistency coefficient (m={1,5,10,20}) on pressure and density along the centerline is examined in Figure 8 for power-law index values n=0.5 and n=1.5. As illustrated in the figure, with increasing m both p and ρ also increase in each region. However, this behavior is more pronounced for n > 1 (shear-thickening fluids), since the m dependent behavior on the viscosity scaling ratio dominates in shear-thickening regime compared to shear-thinning one [43].

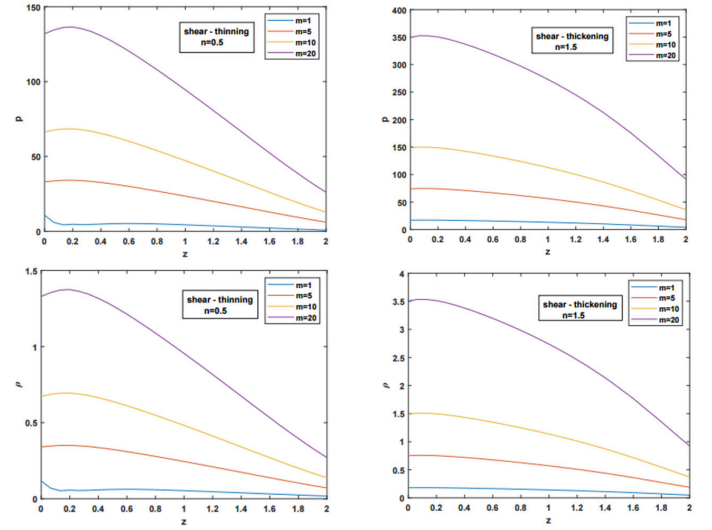

Figure 8. Influence of variation m on pressure and density

5.2. The relationship between viscosity and shear rate with n and m variation

Is that the viscosity (μ_s) is directly proportional to the shear rate (γ), as shown in Equation 8. The influence of n on this relationship is shown in Figure 9, which demonstrates three regimes based on the value of n. When the shear rate n < 1 increases the fluid exhibits its shear-thinning behavior, meaning that the viscosity decreases. This intriguing phenomenon results from entanglements among polymer chains that form when they are incorporated into the fluid, before they flow together. These entanglements break at higher shear rates, allowing chains to align and molecular mobility to increase, which ultimately reduces viscosity. On the other hand, n > 1 the flu-

id exhibits shear-thickening behavior, in which viscosity increases with shear rate. The fluid behaves as a Newtonian fluid, n=1 with a viscosity that does not vary with the applied shear rate. For additional insights, see [44].

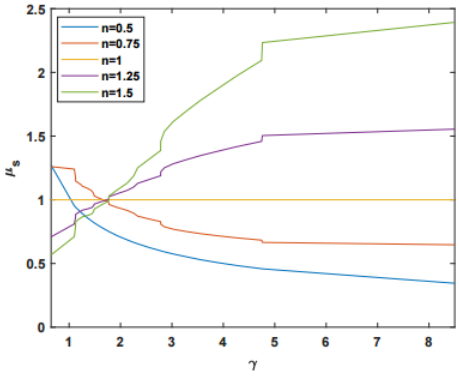

Figure 9. Influence of variationn on relation between viscosity & shear rate

The consistency coefficient (m) is one of the key parameters in controlling the interaction between viscosity and shear rate. In particular, its influence scales when n > 1 with m, scaling greatly increases the fluid's aversion to flow. In the opposite direction, for n < 1 , the intrinsic shear-thinning property of fluid with its viscosity declining along with rising shear rate renders m effect infirm [45]. Figure 10 illustrates this behavior.

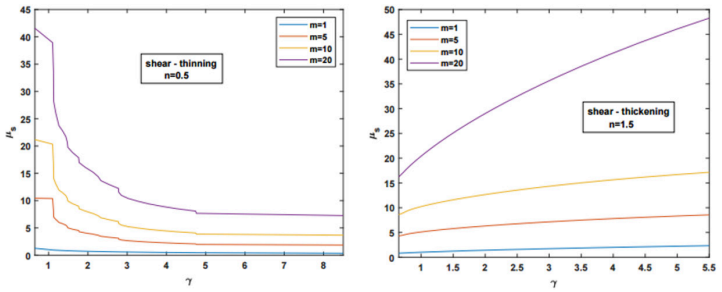

Figure 10. Influence of variation m on relation between viscosity & shear rate

5.3. Temperature profiles with n and m variations

Show that, in compressible fluids, the effect of the n on temperature (T) is more robust than that in incompressible fluids. As shown in Figure 11, higher values generate higher temperature; this effect is more pronounced in compressible fluids. This increased sensitivity is due to the more complex interdependence between pressure and temperature in compressible fluids, which leads to large temperature-induced changes in parameters such as viscosity (or, more broadly, rheology). In comparison, the relationship between these quantities becomes an easier expression and has a less signification impact on fluid physical properties for incompressible fluids as presented in [46].

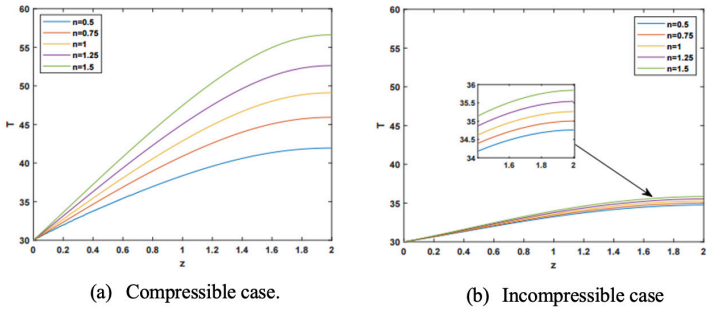

Figure 11. Comparison of the effect of the variation of n on the temperature in the compressible and incompressible states

As with n, the effect of m on temperature exhibits a similar trend, though is most significant in compressible fluids. The reason for this is that in compressible fluids density varies considerably with pressure and temperature variations. Therefore, temperature also has significant effect of the consistency coefficient, which is a measure of fluid's viscosity. However, for incompressible fluids the density is much less affected by temperature changes leading to a two order of magnitude lower dependence of the consistency coefficient on temperature [47]. Observing Figure 12, an increment of m produces a big jump in temperature which is more noticeable for shear-thickening fluids (n=1.5), harsher values of m means that the viscosity raised. Furthermore, it is noted that the influence of m on temperature is more significant in compressible fluids than incompressible fluids.

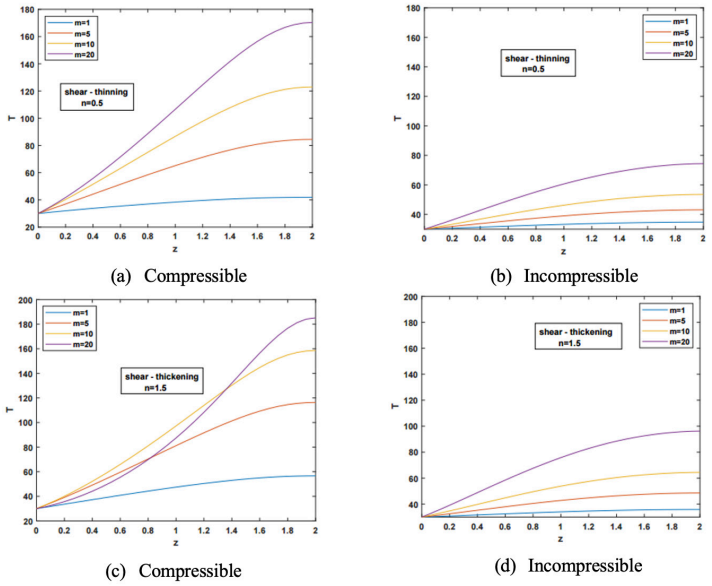

(a) Compressible (b) Incompressible

(c) Compressible (d) Incompressible

Figure 12. Comparison of the effect of the variation of m on the temperature in the compressible and incompressible states

5.4. For temperature profiles with k and Pr variation in system of non-isothermal flow

Thermal conductivity (k) and the Prandtl number (Pr) are key parameters that have a major impact on temperature distribution and heat transfer characteristics. The current study examines the parameters p and Pr, in the range of 0.6≤k=Pr≤1.4 with 0.2 bark steps of, by fixing the value of m=1. Data were analyzed for two power-law indices (n = 0.5), (n = 1.5): shear-thinning and shear-thickening. The results are then compared with those of the incompressible flow case to investigate the effects of these parameters on changes in the thermal and flow fields. The results from comparing the thermal properties with fluid characteristics under different rheological conditions allow insight into the interaction of those properties. For compressible and incompressible fluids, the effect of k on T is depicted in Figure 13 for two values of the power-law index (n=0.5,n=1.5). From the results, we can see that as k decreases, T tends to increases for compressible fluids especially at n = 1.5, as noted by [35].

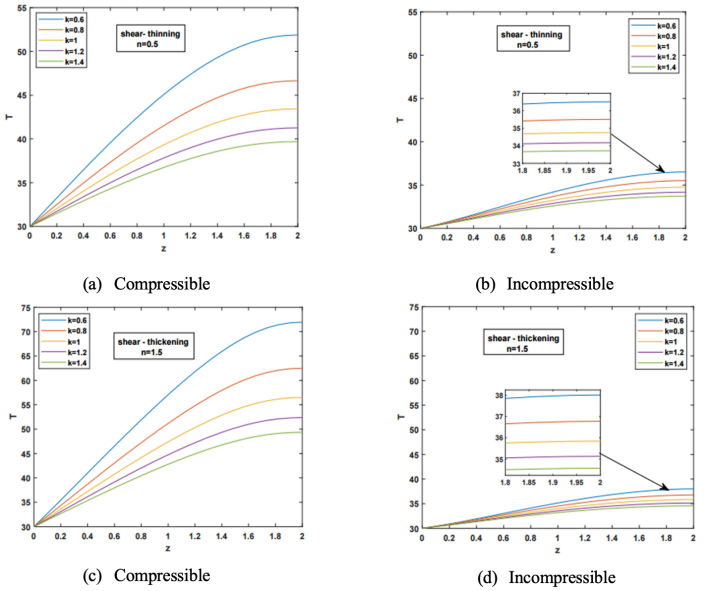

(a) Compressible (b) Incompressible

(c) Compressible (d) Incompressible

Figure 13. Comparison of the effect of the variation of k on the temperature in the compressible and incompressible states

As also is the case for thermal conductivity (k) the Prandtl number (Pr) modifies temperature profiles in a similar manner. As illustrated in Figure 14, a decrease of Pr results in an increase of temperature. In particular, as shown in [35], the effect is more significant and pronounced for n=1.5 in the case of compressible fluids.

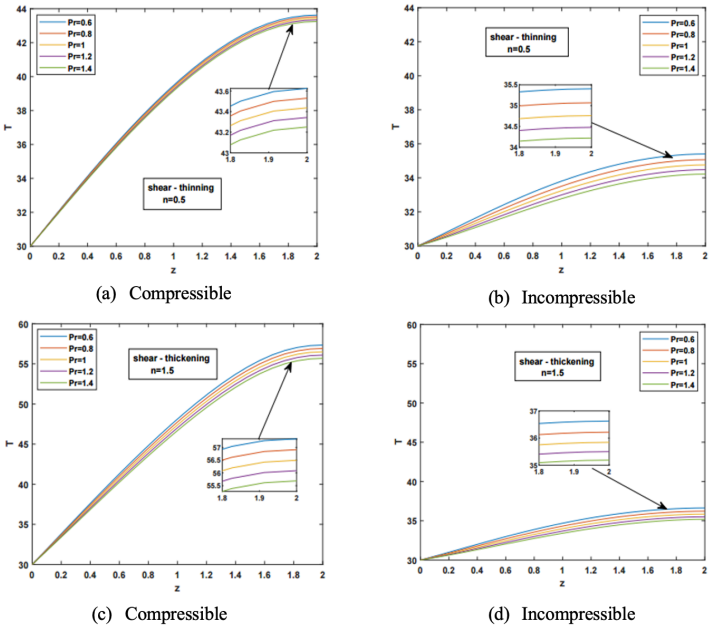

(a) Compressible (b) Incompressible

(c) Compressible (d) Incompressible

Figure 14. Comparison of the effect of the variation of Pr on the temperature in the compressible and incompressible states.

5.5. Shear stress and normal stress with n and m variation

Finally, we explore the impact of n and m on shear stress (τ_{rz}) and normal stress (τ_{zz}) as shown in Figures 15, 16, and 17. Figure 15 shows that the magnitudes of the shear and normal stresses increase, consistent with the shear-thickening behavior of the fluid. These results are consistent with those reported previously [48-51]. When m varies, Figures 16 and 17 show the effects on n = 0.5 and n = 1.5, respectively. The trend shows that the magnitudes of τ_{rz} and τ_{zz} increase with m shear-thickening fluids clearly following this pattern. This phenomenon is caused by the increased viscosity for larger values of m (as noted in [43]).

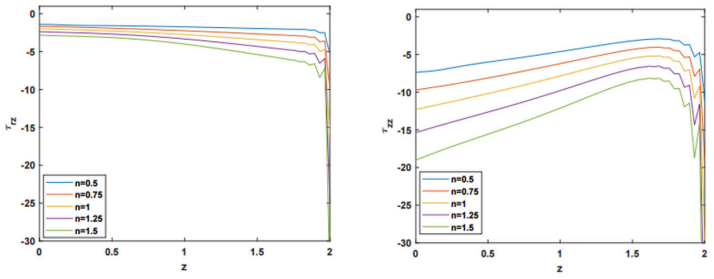

Figure 15. Influence of variation n on τ_{rz} and τ_{zz}

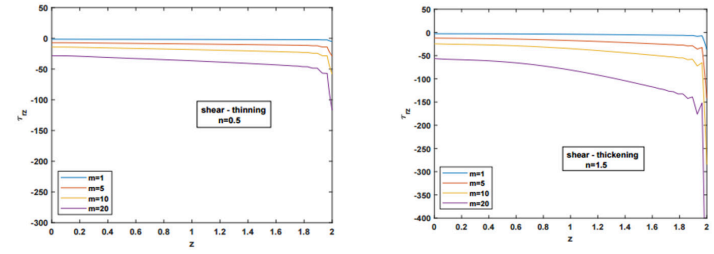

Figure 16. Influence of variation m on τ_{rz}

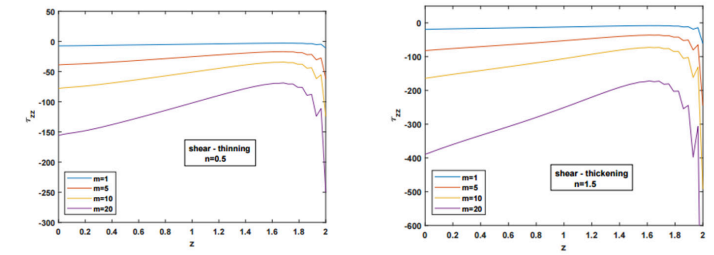

Figure 17. Influence of variation m on τ_{zz}

6. Conclusion

This study successfully extends the developed Taylor-Galerkin/Pressure-Correction method to simulate compressible, inelastic, non-Newtonian fluid flows under non-isothermal conditions in cylindrical coordinates. This approach accounts for the full coupling of momentum, energy, and mass transport due to compressibility, and provides a direct solution to the energy equation via a two-step Lax-Wendroff scheme. Numerical methods have been shown, through quantitative analyses, to be robust and accurate. At the channel outlet, increasing the power-law index from n=0.5 (shear-thinning) to n=1.5 (shear-thickening) caused a reduction in flow velocity by up to, indicating 10% increased flow resistance. For shear-thickening fluids, increasing the consistency coefficient led m=1 to m=20 an 35% increase in outlet velocity, while shear-thinning flows showed 10% a smaller increase due to lower viscosity sensitivity. Pressure (p) and density (ρ) profiles at the pipe centerline showed a peak pressure of approximately 400 and 4 at n=1.5 and m=20 for shear-thickening fluids, indicating that both parameters are strongly related to flow resistance. Likewise, shear and normal stresses increased by as much as 50% with increasing n and m, highlighting their effect on the fluid stress state. Thermal findings demonstrate that, particularly in compressible flows, the temperature increases 20% as the Prandtl number and thermal conductivity decrease. The temperature at the channel outlet T=180 was higher in shear-thickening m=20 fluids, demonstrating the strong coupling between viscosity and thermal diffusion. The novelty of this work lies in extending the capabilities of the Taylor-Galerkin/Pressure-Correction scheme developed for power-law fluids to include compressibility and non-isothermal effects, which have not previously been addressed in this context. It is suitable for simulating realistic industrial processes involving polymer melts, geophysical flows, or high-speed thermally driven systems. Possible future work includes extending the framework to three-dimensional domains, transient flow regimes, and viscoelastic fluid models. Further development of tailored turbulence models and aggressive mesh adaptation strategies will improve simulation fidelity for a range of engineering applications.

Copyright permission statement

All figures included in this manuscript are original works created by the authors. No copyrighted figures, images, or graphical elements from other sources have been used in this manuscript.

Nomenclature

v_r	Velocity in - direction
v_z	Velocity in -direction
ρ	Fluid's density
μ_s	Solvent viscosity
p	Pressure of fluid
T	Fluid temperature

t	Time
C_p	Thermal heat capacity
k	Thermal conductivity
Φ	Dissipation function
m	Consistency parameter
n	Power-law index
γ	Shear rate
V^0	Characteristic velocity
p^0	Characteristic pressure
ρ^0	Characteristic density
T_0	Characteristic temperature
ΔT	Reference temperature difference
Re	Reynolds number
Pr	Prandtl number
Ec	Eckert number
$c^2(x,t)$	Speed of sound
τ_{rz}	Shear stress
τ_{zz}	Normal stress

References

[1] Rohsenow WM, Hartnett JP, Cho YI. Handbook of Heat Transfer. Volume 3. New York: McGraw-Hill; 1998.

[2] Wu WT, Massoudi M. Recent advances in mechanics of non-Newtonian fluids. Fluids 2020;5(1). https://doi.org/10.3390/fluids5010010.

[3] Sadiq N, Jawad M, Khalid F, Jahan S, Hassan AM. Comparative analysis of non-Newtonian and Newtonian fluid flow with dual slip in the presence of motile microorganisms and nanoparticles. BioNanoScience 2024;14(2):1504-1519. https://doi.org/10.1007/s12668-023-01284-x

[4] Gupta S, Sharma PK, Kumar S, Tiwari CM. Influence of buoyancy forces in MHD non-Newtonian convective nanofluid utilizing Buongiorno's model induced by 3D exponential sheet. J Therm Eng 2024;10(5):1107-1119.https://doi.org/10.14744/thermal.0000854

[5] Mansour A, Chigier N. Air-blast atomization of non-Newtonian liquids. J Non-Newtonian Fluid Mech 1995;58(2):161-194. https://doi.org/10.1016/0377-0257(95)01356-Z

[6] Shin JH, Lee I, Kim H, Koo J. Spray atomization and structure of supersonic liquid jet with various viscosities of non-Newtonian fluids. Open J Fluid Dyn 2012;2(4):297-304.https://doi.org/10.4236/ojfd.2012.24A036

[7] Mansour MH, Kawahara A, Sadatomi M. Experimental investigation of gas-non-Newtonian liquid two-phase flows from T-junction mixer in rectangular microchannel. Int J Multiph Flow 2015;72:263-274.https://doi.org/10.1016/j.ijmultiphaseflow.2015.02.019

[8] Santoso A, Goto D, Takehira T, Aslam A, Kawahara A, Sadatomi M. Non-Newtonian two-phase flow characteristics across sudden expansion in horizontal rectangular minichannel. World J Mech 2016;6(8):257-272.https://doi.org/10.4236/wjm.2016.68021

[9] Gkotsis PK, Evgenidis SP, Karapantsios TD. Influence of Newtonian and non-Newtonian fluid behaviour on void fraction and bubble size for a gas-liquid flow of sub-millimeter bubbles at low void fractions. Exp Therm Fluid Sci 2019;109:109875. https://doi.org/10.1016/j.expthermflusci.2019.109912

[10] Sepulveda J, Montillet A, Della Valle D, Loisel C, Riaublanc A. Deformation of gas-liquid interfaces in a non-Newtonian fluid at high throughputs inside a microfluidic device and effect of an expansion on bubble breakup mechanisms. Chem Eng Sci 2020;213:115413.https://doi.org/10.1016/j.ces.2019.115377

[11] Shateri A, Mirzagoli Ganji A, Jalili P, Jalili B, Domiri Ganji D. Utilizing python for numerical analysis of bioconvection in magnetized Casson-Maxwell nanofluid systems with gyrotactic microorganisms: An investigation of dominant factors. Results Eng 2025;25:1-11.https://doi.org/10.1016/j.rineng.2024.103760

[12] Azar AA, Jalili P, Jalili B, Ganji DD. The comprehensive analysis of magnetohydrodynamic Casson fluid flow with rectangular porous medium through expanding/contracting channel. Multidiscip Model Mater Struct 2025;21(1):68-97. https://doi.org/10.1108/MMMS-07-2024-0179

[13] Mahboobtosi M, Jalili B, Shateri A, Jalili P, Domiri Ganji D. Heat transfer characteristics in the squeezing flow of Casson fluid between circular plates: A comprehensive study. Adv Mech Eng 2024;16(10):1-11.https://doi.org/10.1177/16878132241290942

[14] Nadalinia Chari F, Jalili P, Jalili B, Domiri Ganji D. MHD Casson non-Newtonian fluid flow in a channel with expanding/contracting porous walls in the presence of thermal radiation. Proc Inst Mech Eng Part E J Process Mech Eng 2024;1-11. https://doi.org/10.1177/09544089241241459

[15] Roshani H, Jalili P, Jalili B, Ahmad I, Hendy AS, Ali MR, Ganji DD. The effect of magnetic field on the heat transfer in the porous medium octagonal cavity with Cassini oval barriers. Case Stud Therm Eng 2024;56:1-11.https://doi.org/10.1016/j.csite.2024.104194

[16] Jalili B, Sadinezhad Fard M, Khan Y, Jalili P, Ganji DD. A novel technique to analyze the fractional model of Williamson and Casson non-Newtonian boundary layer flow. Multidiscip Model Mater Struct 2024;20(2):279-294.https://doi.org/10.1108/MMMS-09-2023-0309

[17] Jalili B, Rezaeian A, Jalili P, Domiri Ganji D, Khan Y. Squeezing flow of Casson fluid between two circular plates under the impact of solar radiation. ZAMM Z Angew Math Mech 2023;103(9):1-11.https://doi.org/10.1002/zamm.202200455

[18] Sadinezhad Fard M, Torabiyan A, Jalili P, Jalili B, Domiri Ganji D. Investigating the magnetohydrodynamics non-Newtonian fluid movement on a tensile plate affected by variable

thickness with Dufour and Soret effects: Akbari Ganji and finite element methods. Int J Electrochem Sci 2024;19(8):1-11. https://doi.org/10.1016/j.ijoes.2024.100701

[19] Ozsahin DU, Jalili B, Asadi Z, Shateri A, Jalili P, Domiri Ganji D, Ahmad H, Nofal TA. Investigation of turbine cooling using semi-analytical methods in non-Newtonian fluid flow with porous wall. Case Stud Therm Eng 2024;53:1-11.https://doi.org/10.1016/j.csite.2023.103808

[20] Makkar V, Poply V. Impact of outer velocity on flow, heat, and mass transfer of Casson nanofluid over a non-linear stretching sheet. J Therm Eng 2021;7(6):1353-1365.https://doi.org/10.18186/thermal.859221

[21] Ramachandra Prasad V, Abdul Gaffar S, Keshava Reddy E, Anwar Bg O. Numerical study of non-Newtonian Jeffreys fluid from a permeable horizontal isothermal cylinder in non-Darcy porous medium. J Braz Soc Mech Sci Eng 2015;37(6):1765-1783.https://doi.org/10.1007/s40430-014-0301-5

[22] Sarojamma G, Sreelakshmi K, Animasaun IL. Numerical study of nonlinear thermal radiative heat transfer in a non-Darcy chemically reactive Casson fluid flow. SN Appl Sci 2019;1(10):1-11.https://doi.org/10.1007/s42452-019-1159-z

[23] Chang A, Sun HG, Vafai K, Kosari E. Numerical analysis of flow and forced convection heat transfer of non-Newtonian fluid in a pipe based on fractional constitutive model. Int J Numer Methods Heat Fluid Flow 2021;31(8):2680-2697. https://doi.org/10.1108/HFF-10-2020-0637

[24] Ren X, Xin Z, Liu F. A non-Newtonian thermal lattice Boltzmann method for simulation of Rayleigh-Bénard convection of power-law fluids. AIP Adv 2023;13(11):1-11.https://doi.org/10.1063/5.0168404

[25] Chtaibi K, Hasnaoui M, Ben Hamed H, Dahani Y, Amahmid A. Numerical simulations of the Lorentz force effect on thermal convection in an inclined square cavity filled with a non-Newtonian fluid. Lect Notes Mech Eng 2024:196-206. https://doi.org/10.1007/978-3-031-43934-6_21

[26] Vamsi BVSR, Raveendiran P, Sastry MRC. Experimental and numerical study of fluid flow and heat transfer in the impinging of inline round jets. J Therm Eng 2025;11(1):270-289. https://doi.org/10.14744/thermal.0000918

[27] Hawken DM, Tamaddon-Jahromi HR, Townsend P, Webster MF. A Taylor-Galerkin-based algorithm for viscous incompressible flow. Int J Numer Methods Fluids 1990;10(3):327-351.https://doi.org/10.1002/fld.1650100307

[28] Tamaddon-Jahromi HR, Ding D, Webster MF, Townsend P. A Taylor-Galerkin finite element method for non-Newtonian flows. Int J Numer Methods Eng 1992;34(3):741-757.https://doi.org/10.1002/nme.1620340304

[29] Carew EOA, Townsend P, Webster MF. A Taylor-Petrov-Galerkin algorithm for viscoelastic flow. J Non-Newtonian Fluid Mech 1993;50(2-3):253-287.https://doi.org/10.1016/0377-0257(93)80034-9

[30] Ngamaramvaranggul V, Webster MF. Computation of free surface flows with a Taylor-Galerkin/Pressure-Correction algorithm. Int J Numer Methods Fluids 2000;33(7):993-1026.https://doi.org/10.1002/1097-0363(20000815)33:7<993::AID-FLD40>3.0.CO;2-A

[31] Al-Muslimawi AH. Theoretical and numerical studies of die swell flow. Korea Aust Rheol J 2016;28(3):229-236.https://doi.org/10.1007/s13367-016-0023-6

[32] Sharhan A, Al-Muslimawi A. Inelastic solution for power law fluid with Taylor-Galerkin/Pressure-Correction finite element method: Axisymmetric contraction flows. J Appl Fluid Mech 2023;16(12):2411-2423.https://doi.org/10.47176/jafm.16.12.1982

[33] Al-Haboobi A, Al-Juaifri GA, Al-Muslimawi AH. Numerical study of Newtonian laminar flow around circular and square cylinders. Results Control Optim 2024;14:1-11.https://doi.org/10.1016/j.rico.2023.100328

[34] Al-Haboobi A, Fadhel IA, Sharhan AA, Al-Muslimawi AH. Computational simulation of compressible Newtonian flow past circular and square bluff bodies. Ocean Syst Eng 2024;14(4):315-330.https://doi.org/10.12989/ose.2024.14.4.315

[35] Al-Haboobi A, Al-Muslimawi AH. Novel algorithm for compressible Newtonian axisymmetric thermal flow. Int J Mod Phys C 2024;35(3):1-11.https://doi.org/10.1142/S0129183124500256

[36] Shapovalov VM. On the applicability of the Ostwald-De Waele model in solving applied problems. J Eng Phys Thermophys 2017;90(5):1213-1218.https://doi.org/10.1007/s10891-017-1676-9

[37] Al-Haboobi A, Al-Muslimawi AH. A new algorithm for solving thermal Newtonian flow in axisymmetric straight channel. Basrah J Sci 2023;41(3):399-418.https://doi.org/10.29072/basjs.20230301

[38] Dymond JH, Malhotra R. The Tait equation: 100 years on. Int J Thermophys 1988;9(6):941-951.https://doi.org/10.1007/BF01133262

[39] Heuz T. Lax-Wendroff schemes for elastic-plastic solids. J Comput Phys 2019;396:89-105.https://doi.org/10.1016/j.jcp.2019.06.050

[40] Crank J, Nicolson P. A practical method for numerical evaluation of solutions of partial differential equations of the heat-conduction type. Adv Comput Math 1996;6(1):207-226. https://doi.org/10.1007/BF02127704

[41] Westermaier S, Kowalczyk W, et al. Implementation of non-Newtonian fluid properties for compressible multiphase flows in OpenFOAM. Open J Fluid Dyn 2020;10(02):135. https://doi.org/10.4236/ojfd.2020.102009

[42] Ikoku CU, Ramey Jr HJ. Transient flow of non-Newtonian power-law fluids in porous media. Soc Pet Eng J 1979;19(03):164-174.https://doi.org/10.2118/7139-PA

[43] Pang B, Wang S, Chen W, Hassan M, Lu H. Effects of flow behavior index and consistency coefficient on hydrodynamics of power-law fluids and particles in fluidized beds. Powder Technol 2020;366:249-260.https://doi.org/10.1016/j.powtec.2020.01.061
[44] Gooch JW, editor. Power law (Ostwald-DeWaele model). In: Springer Handbook of Experimental Fluid Mechanics. Springer New York; 2007. p. 781.https://doi.org/10.1007/978-0-387-30160-0_9193
[45] Koponen AI. The effect of consistency on the shear rheology of aqueous suspensions of cellulose micro- and nanofibrils: a review. Cellulose 2020;27(4):1879-1897.https://doi.org/10.1007/s10570-019-02908-w
[46] Prasad D, Subrahmanyam SV, Panda SS. Thermal, squeezing and compressibility effects in lubrication of asymmetric rollers. Tribol Ind 2014;36(3):244–258.
[47] Dak M, Verma RC, Jaaffrey SNA. Rheological properties of tomato concentrate. Int J Food Eng 2008;4(7):1-11.https://doi.org/10.2202/1556-3758.1470
[48] Tripathi S. Effects of power law fluid characteristics on core-annular flow in a horizontal pipe. Lect Notes Mech Eng 2024:77-84.https://doi.org/10.1007/978-981-99-6074-3_8
[49] Keslerov R, Kozel K. Numerical modelling of incompressible flows for Newtonian and non-Newtonian fluids. Math Comput Simul 2010;80(8):1783-1794.https://doi.org/10.1016/j.matcom.2009.12.005
[50] Jeong SW, Leroueil S, Locat J. Applicability of power law for describing the rheology of soils of different origins and characteristics. Can Geotech J 2009;46(9):1011-1023.https://doi.org/10.1139/T09-031
[51] Siddiqui AM, Ahmed M, Ghori QK. Couette and Poiseuille flows for non-Newtonian fluids. Int J Nonlinear Sci Numer Simul 2006;7(1):15-26.https://doi.org/10.1515/IJNSNS.2006.7.1.15